# Simulation and analysis of solenoidal ion sources

A. R. Alderwick, A. P. Jardine,* H. Hedgeland, D. A. MacLaren,† W. Allison, and J. Ellis

*Cavendish Laboratory, University of Cambridge, JJ Thomson Avenue, Cambridge, CB3 0HE, United Kingdom*

We present a detailed analysis and simulation of solenoidal, magnetically confined electron bombardment ion sources, aimed at molecular beam detection. The aim is to achieve high efficiency for singly ionized species while minimizing multiple ionization. Electron space charge plays a major role and we apply combined ray tracing and finite element simulations to determine the properties of a realistic geometry. The factors controlling electron injection and ion extraction are discussed. The results from simulations are benchmarked against experimental measurements on a prototype source.

## I. INTRODUCTION

High sensitivity mass spectrometers are important in many branches of research and industry, ranging from ultra-high vacuum diagnostics to biological analysis. Many designs exist, but it is usually the efficiency of the ion source that limits sensitivity(1). In the present work, we are concerned with understanding and improving the design of high-efficiency ion sources for atomic beams, particularly those used in helium atom scattering experiments, where a high ionization efficiency must be combined with a low background from ionized residual gas(2; 3) and where high time resolution of detection is not critical. We limit discussion to electron bombardment ion sources, the most common type, where the principle of operation is that a region containing energetic electrons is overlapped with the atoms or molecules to be ionized.

Over the past 50 years, several electron bombardment ion sources for molecular beam detection have been described and a useful overview is given by Bassi(4). Many devices are based on the early design of Nier(5), which allows the atomic or molecular beam to intersect the electron beam orthogonally, in a small volume, producing ions with well defined positions, velocities and energies. The ionization efficiency of such a device can be improved in only two ways: either by increasing the ionization volume or by increasing the density of electrons. There are clear limits to both of these approaches.

Designs of the Weiss and Brink type(6; 7) have a larger volume of overlap between the electrons and the molecular beam. Here, fine grids along the length of the source define the ionization region and electrons are supplied through the sides of the grid. The axis of the device can be arranged to coincide with the axis of the molecular beam to increase the total probability of ionization. Electrons can achieve multiple passes through the molecular beam; however, the difficulty of manufacture of long, high-transparency grids and in providing a uniform source of electrons along the entire device imposes constraints on the length. Increasing the density of electrons, for example by confining the electron motion in a magnetic field(8; 9) also improves the efficiency but the resulting space charge makes ion extraction problematic, especially for a long device. In practice, ionizers of the Weiss and Brink type are rarely more than a few centimeters in length and in the present work we seek to increase that figure by an order of magnitude.

Many of the above constraints can be overcome by retaining the cylindrical geometry and coincidence of the molecular beam and ionizer, but also supplying electrons co-axially, from one end of the device(10–14). A solenoidal magnetic field is used to confine the electrons and hence the ionization volume is defined by the magnetic field rather than by transparent grids. Injection of electrons along the solenoid axis allows the overlap between electrons and atoms to be increased almost indefinitely, as we show below. Careful design and the elimination of electron loss mechanisms enables the construction of long ion sources (typically 300 mm) that require relatively small power input to the cathode. Operation of axially extended ion sources relies on electron space charge to confine the ions radially, and some of the engineering difficulties are similar to those in electron beam ion sources used for the production of highly ionized ion beams(1; 15); however, in the present design the aim is to facilitate rapid ion extraction and minimize the opportunity for multiple electron-atom collisions.

Solenoidal ion sources have been demonstrated to have ultra-high efficiency(11), but their exploitation can be limited by an extreme sensitivity to design factors such as the means of electron injection and ion extraction(12). The aim of the present work is to consider these two key aspects of operation in some detail. We simulate 3-dimensional electron trajectories and, by including the effects of electron space charge, we show the factors that give efficient electron injection. The trajectories lead to an accurate, self-consistent electrostatic potential in which the ion motion and extraction can be understood. In addition, we present some simple measurements using a prototype design that illustrates many of the simulated effects.

## II. MAGNETICALLY CONFINED ELECTRON BOMBARDMENT ION SOURCES

The principal components of a solenoidal ion source are shown in Fig. 1. The solenoid winding, **1**, produces a magnetic field (dotted lines). The winding also defines the axis of the device and surrounds a "liner", **2**, which determines the electrical boundary conditions for the motion of both electrons and ions. Electrons originate at the cathode, **3**, which

*Corresponding author; Electronic address: apj24@cam.ac.uk

†Present address: Department of Physics & Astronomy, Kelvin Building, University of Glasgow, Glasgow, G12 8QQ, United Kingdom

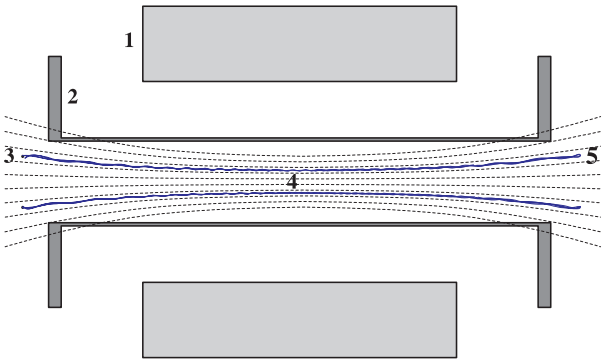


FIG. 1 [Color online] Schematic cross-section of a solenoidal ion source. The main features are: **1**, the solenoid winding to create a magnetic field (dotted lines); **2**, a conducting liner defining the electrical boundary conditions and providing the core of the ion source; **3**, the cathode to provide electrons that follow helical trajectories through the core region, **4**. Typical trajectories are shown as solid (blue) lines and the the electric fields are such that they reflect at the far end, **5** (see text).

in this case is simply a fine, circular filament, coaxial with the liner. A potential difference, usually of a few hundred volts, is applied between the cathode and liner, and both are usually raised to a potential above that of their surroundings so that the energy of the ions, after extraction, is convenient for subsequent mass analysis. Electrons are therefore accelerated from the cathode into the core of the device, **4**; and in the low emission limit, when there is negligible electric field, execute helical trajectories around the magnetic field lines. With significant electron currents, the electric field due to the space charge (as outlined below) acts radially outwards. In the presence of the axial magnetic field, it causes the central lines of the helix-like trajectories to describe their own helices around the solenoid axis. Critically, the space charge does not cause the electron trajectories to diverge and as a result, in the absence of collisions, the electron trajectories remain confined indefinitely, allowing solenoids of arbitrary length to be used. In the case of a strong magnetic field, the radius of the helical trajectories is small and the electrons form a hollow cylinder(16), with the electron density concentrated around the magnetic field lines that pass through the filament. As the electrons emerge at the far end of the device, **5**, their motion can be reversed providing the filament potential is greater than the potential of the surroundings. In the absence of loss mechanisms, the ion source operates in a reflex mode of operation(15), in which the electrons perform a return journey back to the vicinity of the filament, and are capable of traveling back and forth indefinitely. It follows that, if ionization is the only loss mechanism for electrons, many oscillations will occur so that a large electron space charge will be created near the filament and further emission of electrons will be suppressed. Under such idealized conditions, the emission current from the cathode will drop to a very low value, and the filament will operate in a space charge limited regime. For this reason, it is more convenient to characterize the behavior of a solenoidal ion source in terms of the total charge held within the device rather than by the emission current from the filament. The ideal behavior is, therefore, quite different from that of a Brink type ion source(7), where emission is the key parameter.

We introduce the main principles of operation of the device using a simple analytic model for the space charge before discussing the details using accurate, self-consistent calculations for the electron behavior (Section V). As discussed above, electron emission from a well-positioned circular filament placed at the entrance of a solenoid will give rise to a tubular electron cloud within the bore of the solenoid. It can be shown that at any point in the core of the device, the inner and outer radii of this tubular electron cloud are proportional to $B(z)^{-1/2}$, where $B(z)$ is the magnetic field strength at axial position $z$. It is most convenient to describe the electron cylinder by its outer radius, $r_c$, and the ratio of inner to outer radius, $\alpha$, $(0<\alpha<1)$. The outer radius, $r_c$, is a function of $z$ while $\alpha$ is constant. At any axial position within the solenoid, an estimate for the radial potential is then given by applying Gauss's Law to a long hollow cylinder of charge. If the hollow cylinder has a uniform volume charge density, $\rho=\lambda/\left[\pi r_c^2\left(1-\alpha^2\right)\right]$, where $\lambda$ is the charge per unit length (negative for a beam of electrons), then the potential $V(r)$ at radius $r$ is

$$V(r)=V_L+\begin{cases}\frac{\lambda}{2\pi\varepsilon_0}\ln\frac{r_L}{r} & r_c\le r\le r_L\\ \frac{\lambda}{2\pi\varepsilon_0}\left(\ln\frac{r_L}{r_c}+\frac{r_c^2-r^2}{2r_c^2(1-\alpha^2)}+\frac{\alpha^2}{1-\alpha^2}\ln\frac{r}{r_c}\right) & \alpha r_c\le r<r_c\\ \frac{\lambda}{2\pi\varepsilon_0}\left(\ln\frac{r_L}{r_c}+\frac{1}{2}+\frac{\alpha^2}{1-\alpha^2}\ln\alpha\right) & 0\le r<\alpha r_c\end{cases} \quad (1)$$

Here, $r_L$ and $V_L$ are the radius and electric potential of the liner respectively and $r_c$, as described above, is a function of $z$. The lines in Fig. 2 illustrate the form of the resulting electric potential and the shaded region indicates the radial extent of the corresponding tubular electron beam. In the absence of significant electron space charge, the electrostatic potential is given by the liner potential ($V_L$, the fine, horizontal line), while in the presence of an electron space charge a flat-bottomed, radial potential well is created (bold, solid line). For a particular electron density, the axial potential well depth,

$$V_L-V(0)=-\frac{\lambda}{2\pi\varepsilon_0}\left(\ln r_L-\ln r_c+\frac{1}{2}+\frac{\alpha^2}{1-\alpha^2}\ln\alpha\right), \quad (2)$$

depends on the radius of the liner, $r_L$, and the (z-dependent) radius of the electron beam, $r_c$. Both properties are varied in the designs below in order to control the ion dynamics. In particular, $r_L$ is decreased to raise the potential and prevent the unwanted escape of ions while a decrease in $r_c$, achieved by modifying the magnetic field, reduces the potential and facilitates ion extraction.

Gas ionization can occur anywhere within the electron cloud, indicated by the shaded regions of Fig. 2. If the initial energy of the ion is neglected, then the energy spread of the ionized atoms will correspond to the potential variation in that region. Substitution into Eq. 1 gives the ion energy-spread, $S$, as

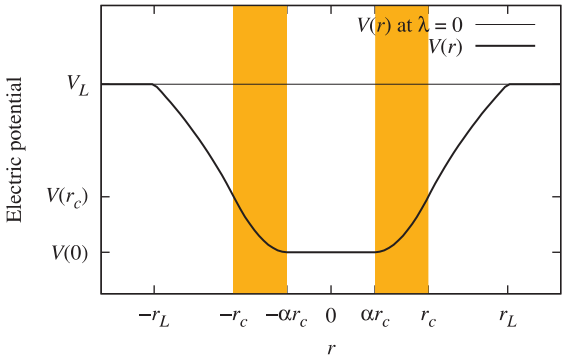


FIG. 2 Radial variation of the electric potential, $V(r)$, inside a long solenoid ion source with (thick line) and without (thin line) space charge, given by Eq. 1. In the absence of space charge ($\lambda = 0$), the potential is simply that of the liner, $V_L$. In general, $\lambda < 0$ and a hollow, cylindrical cloud of electrons forms between within the shaded region ($\alpha r_c < r < r_c$). Ionization also occurs within the shaded region and the variation of potential gives an ion energy spread of $V(r_c)$–$V(0)$. The value of $\alpha$ is chosen to be 0.45 so that the functional form is illustrated clearly.

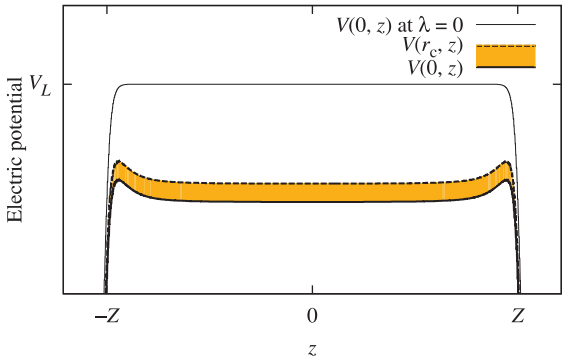


FIG. 3 Longitudinal variation of the electric potential, $V(r,z)$, inside a solenoid ion source of length $2Z$. In the absence of space charge ($\lambda = 0$), the axial potential $V(0,z)$ (thin solid line) is $V_L$ and swiftly decays outside the liner. In the presence of space charge ($\lambda < 0$, shaded region), the reduction in magnetic field strength at the ends of the solenoid causes $r_c$ to increase and leads to the formation of potential barriers (see text). Of particular interest is $V(0,z)$ (thick solid line), which describes the depth of the space charge potential well, and $V(r_c,z)$ (thick dashed line): together they describe the range of ion energies produced (shaded region) at each point along the solenoid.

$$S = V(r_c) - V(\alpha r_c) = V(r_c) - V(0) = -\frac{\lambda}{2\pi\varepsilon_0}\left(\frac{1}{2} + \frac{\alpha^2}{1-\alpha^2}\ln\alpha\right), \quad (3)$$

which depends only on the linear charge density, $\lambda$, and the ratio of inner to outer radii of the electron beam, $\alpha$.

The electron space charge also creates an axial potential well that will confine ions. It follows from the third line of Eq. 1 that inside the core of a uniform solenoid winding, the axial potential depends only on $r_c$, which itself depends on the magnetic field strength, $B(z)$. At both ends of the solenoid $r_c$ increases, as a result of the drop in $B(z)$ due to end effects. $V(0)$ increases in accordance with Eq. 1 and the effect is illustrated in Fig. 3. Here, the thin line indicates the electrostatic potential along the axis in the absence of space charge, while the thick line indicates the potential in the presence of space charge. The space charge creates a potential with a minimum at the center of the solenoid, where the field is strongest, as well as barriers at each end, where the magnetic field lines diverge and the axial field decreases strongly. These barriers act to confine ions within the region of strongest field and highest electron density. Trapping of the ions inside the radial and axial potential well enhances the production of multiply-charged ions and the effect is used in sources for the production of highly-ionized atoms (1; 15; 16). However, in designing a source for detecting atomic beams, the aim is to benefit from the confinement of electrons so as to create a high ionization efficiency per electron, but also to arrange for ions to be extracted quickly and efficiently. We return to the latter topic in Section VI.

The analysis given above illustrates the key points that must be addressed in the design of a high-efficiency detector for atom beams. These are: first, the question of electron injection, which should minimize losses and allow for reflexive trajectories of maximum length; and second, the question of ion extraction, which must prevent trapping by the electron space charge and allow for the rapid removal of singly-ionized particles. Before discussing possible solutions, we describe measurements on a prototype instrument that confirm the importance of these points.

## III. EXPERIMENTAL PROTOTYPE

A prototype ion source was constructed to illustrate the above discussion. The device has a length of approximately 300 mm, which is significantly longer than those described previously (11; 12). In addition, the electron source is simplified, relative to earlier designs, and consists of a simple circular filament immersed in the electrostatic field at the entrance of the liner. The lack of either a repeller electrode or an extraction electrode at the filament, which are common to other designs, is a significant simplification that is discussed in more detail in Section V.

Figure 4 shows the main components of the prototype. The magnetic field strengths at the electron source and the center of the solenoid are 25 mT and 150 mT respectively, which draws the electron beam from the 7 mm diameter filament to a diameter of approximately 3 mm within the solenoid. The 300 mm long solenoid winding, **1**, consists of ten equal layers of rectangular copper wire, 2 mm $\times$ 1 mm, with an operating current of 26.6 A, the construction of which is similar to the solenoids described in Ref. (2). The heat generated by the winding is dissipated by internal and external water cooling (**4**,**5**). Inside the solenoid, a 330 mm long, 12.2 mm inner diameter solenoid liner, **2**, is raised to 1000 V with respect to ground, and the nominal electron energy is chosen as 300 V by setting the cathode, **3**, to 700 V. Two further objects are introduced which break the symmetry of the electrostatic potential between the two ends of the device (Fig. 3), which are

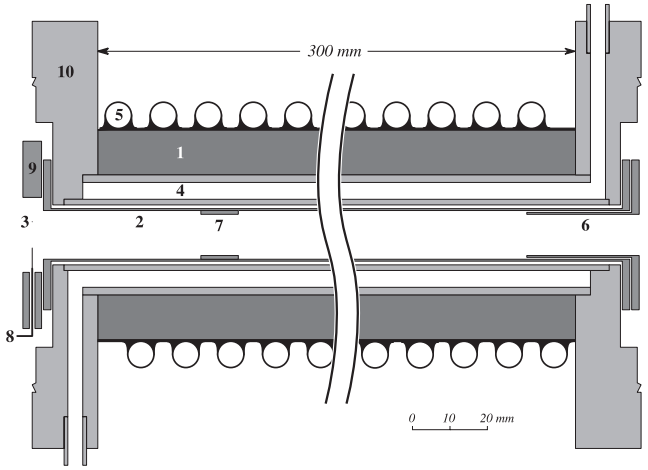


FIG. 4 The prototype solenoidal ion source, to scale, shown as a cross-section through the solenoid axis. All features are composed of stainless steel unless otherwise indicated. The key features are: **1**, solenoid coil wound from 2 mm $\times$ 1 mm copper wire with electrically insulating, thermally conducting epoxy; **2**, solenoid liner; **3**, circular filament made from 0.25 mm diameter tungsten wire and having a radius of 3.5 mm, positioned co-axially with the solenoid and liner and a few millimeters from the solenoid entrance; **4**, internal cooling jacket; **5**, copper external cooling coils; **6**, ion extraction tube, see text; **7**, ion barrier ring, see text; **8**, filament support wires and electrical connections; **9**, filament mounting plate; and **10**, DN63CF ultra-high vacuum flange.

an ion extraction tube, **6**, which is mounted at the exit end and held at a potential 80 V lower than that of the liner to aid extraction; and an optional barrier ring, **7**, inserted near the filament and in contact with the liner to narrow the bore in that region.

Characterization of the ion source is performed using a background gas pressure rather than an atomic beam. A Faraday cup (not shown) is placed just to the right of the ion extraction tube. When set at the same potential as the liner, the Faraday cup collects electrons emitted from the filament after they propagate down the solenoid. Alternatively, if the cup is grounded, it collects any ions that emerge and reflects electrons back into the core of the device, which then operates in a reflexive mode. A second Faraday cup is situated at the cathode end so that any ions emerging from the opposite end can also be measured.

The injection of electrons into the solenoidal field is explored in the data of Table I. Here, measurements of electron current at various points in the system are presented. In all cases, the filament temperature is large enough for emission to be limited by the space charge, rather than thermionic emission. In the first row of the table, the emission current is 34 mA and the Faraday cup at the exit is set to the same potential as the liner, $V_L$. The electron current reaching the cup is 17 mA with the remainder lost to other electrodes. The current lost to the the liner and extraction tube indicates that the filament is not situated ideally, highlighting the importance of accurate filament positioning, which is discussed in detail in Section V. However, sufficient current reaches the Faraday cup to illustrate the role of reflex trajectories and their effect on space-charge near the filament. The effect is illustrated by the second row of Table I. Here, the Faraday cup is set at ground potential so that the electrons that previously reached the cup are reflected. The filament emission current drops immediately to 21.8 mA and there are smaller changes at the liner and extraction tube. The marked drop in emission current ($I_F$ reduces by 12.2 mA) is close to the change in the electron current at the Faraday cup ($I_c$ reduces by 17 mA) and indicates that, in reflexive mode, instead of being collected, electrons simply return to the immediate vicinity of the filament; a result that arises because the magnetic field dominates the electron dynamics. Small changes in the current measured at the liner and extraction tube indicate that the electron trajectories are sensitive to details of the geometry and, in particular, that space charge must be treated self-consistently in any simulation, even at low emission currents. The results also indicate the integrity of the reflexive trajectories and suggest that with careful design, and the elimination of the loss mechanisms evident in Table I, a very low emission current (and a correspondingly low heating power in the filament) should be possible while retaining a high electron density in the ionization region.

| $V_C$ | $I_F$ / mA | $I_L$ / mA | $I_T$ / mA | $I_C$ / mA |
|---|---|---|---|---|
| $V_L$ | 34 $\pm$ 1 | 15 $\pm$ 1 | 2 $\pm$ 1 | 17 $\pm$ 1 |
| 0 | 21.8 $\pm$ 0.1 | 12.5 $\pm$ 0.1 | 9.3 $\pm$ 0.1 | 0 |

TABLE I Measurements of the electron current on various electrodes in the prototype ion source. $I_F$ is the emission current from the filament, $I_L$ is the current reaching the liner, $I_T$ is the current striking the extraction tube, and $I_C$ is the current measured by the Faraday cup at the exit. The currents are shown for two operating potentials, $V_C$, of the Faraday cup. In the first row, the cup has the same potential as the liner, so that all electrons leaving the liner are collected. In the second row, the cup is grounded so that electrons are reflected. The filament current is fixed at 6.47 A throughout.

We now turn to measurements of ion extraction from the prototype device. In this case, the Faraday cups at both ends of the ion source were at ground potential and the ion currents were measured using pico-ammeters. Helium was introduced to a controlled pressure and the sensitivity of the ion source was determined. For these measurements the filament emission current is reduced to a low value, approximately 2 mA, and low gas pressures, $< 10^{-8}$ mbar, are used throughout, in order to minimize any effects arising from ion space charge.

A summary of typical results is given in Table II. Two separate experiments are described: without and with the barrier ring (**7** in Fig. 4). The final column shows the sensitivity obtained by measuring the ion current emerging from each end. Without the barrier ring, most current emerges from the same end as the filament. The result can be understood in terms of the potential barriers created by the electron space charge, shown in Fig. 3. It is clear from Figs. 2 and 3 that ions created at thermal energies cannot leave the liner. Instead, they accumulate until the ion space charge and electron space charge cancel. In the present case, the barrier at the left of the liner

| Barrier ring | Direction | $I_F$/mA ($\pm$0.01) | $I_T$/mA ($\pm$0.01) | Sensitivity (He) /A mbar$^{-1}$ |
|---|---|---|---|---|
| Absent | Forwards | 2.22 | 2.16 | $0.076 \pm 0.001$ |
| Absent | Backwards | 2.21 | 2.16 | $0.267 \pm 0.001$ |
| Present | Forwards | 2.29 | 2.22 | $0.378 \pm 0.003$ |
| Present | Backwards | 2.32 | 2.25 | $0.075 \pm 0.007$ |

TABLE II Ion gauge sensitivity of the prototype ion source, for filament emissions of $\sim$2.25 mA. Faraday cups on either side of the solenoid are grounded via a pico-ammeter to obtain the ion current leaving the ion source past the ion extraction tube (the "forwards" current) and on the filament side (the "backwards" current). Data was collected with and without an ion barrier ring (first column) and using room temperature He gas with total pressures between 35 and $1400 \times 10^{-10}$ mbar. The liner was floated to 1000 V, the extraction tube to 920 V and the filament at 700 V. The current through the filament is 5.00 A, to limit ion space charge in the relatively high pressures used, at which point the maximum emission from the filament is limited by its temperature instead of space charge effects.

must be slightly less than that at the right so that most ions emerge in the backwards direction. The slight difference in barrier heights is most likely due to small manufacturing variations in the solenoid coils at the ends of the device. The presence of a barrier ring changes the situation radically, as shown in the final two rows of Table II. Once the ring is introduced, most current emerges in the forwards direction and the current emerging backwards can be attributed entirely to the atoms ionized between the filament and the barrier ring (see Fig. 4). The barrier ring enhances the local potential by reducing the effective diameter of the liner, $r_L$, thereby manipulating the electron space charge in accordance with Eq. 2. Thus, all ions created to the right of the ring emerge in the forward direction. A similar approach has been used to extract ions by engineering the electron space charge within a uniformly tapered bore (6; 11); however, when an ionization volume of several hundred millimeters in length is desired, a barrier ring is easier to implement than a uniform taper.

Figures for the sensitivity of the device operating as an ion gauge are given in the final column of Table II. The sensitivity of the device when operated as a detector for molecular beams depends on a variety of additional factors, such as the alignment and size of the molecular beam, the overlap of the beam and the electrons and the degree of stagnation, but these figures suggest that high sensitivity is possible, even for species with ionization potentials as high as those in helium.

The results in Tables I and II demonstrate the importance, respectively, of careful injection of electrons and careful extraction of ions. We now examine injection and extraction using trajectory simulations that include the effects of electron space charge. The simulations confirm the analysis of the experimental results given above and indicate how best to design an effective, high-efficiency device.

## IV. NUMERICAL SIMULATION

The length of the device shown in Fig. 4 which incorporates a narrow bore presents a number of challenges to numerical simulation. First, a large number of grid points are required to specify the fields with sufficient precision and, second, efficient methods of trajectory propagation are needed to describe the long, reflexive trajectories that characterize the electron dynamics and space charge. We use two independent software packages to generate the fields and electron trajectories: the *LORENTZ2D-EM* software package(17) and a bespoke program written in-house, both of which exploit the cylindrical symmetry of the device by calculating the electrostatic and magnetostatic fields in a 2-dimensional cylindrical polar geometry.

The electrostatic and magnetostatic fields are first determined in the absence of space charge. The commercial code uses boundary element analysis for both the electric and magnetic calculations, while the in-house code uses finite element analysis and Biot-Savart summation respectively. Both programs then determine the electron space-charge distribution, $\rho(r,z)$, by tracing a series of 3-D electron trajectories through the **E** and **B** fields from an effective cathode, using fourth-order Runge-Kutta numerical integration. In both cases, the trajectories are used to deposit appropriate levels of charge in a grid of finite elements throughout the core of the ion source, depending on the volume represented and the time spent in each element. The electric field is then re-calculated, including the distribution of charges in the finite elements. The process of ray tracing and field solving is repeated to obtain a self consistent solution for a specific number of electrons in the system. For a stable geometry and emission current, $\rho(r,z)$ usually converges after 10–20 iterations.

The main advantage of *LORENTZ2D-EM* is that it uses an irregular mesh with adjustable resolution, which is better able to represent complex geometries, particularly around the filament. The mesh from the in-house program has vertices on a uniform square grid, so that complex geometries are necessarily approximate. However, it is optimized for the speed of trajectory calculation and is at least a factor of 100 faster. The commercial program is limited in the number and length of electron trajectories that can be accommodated in a realistic computing time, whereas the in-house program enables more precise results (through more iterations and a greater number of trajectories) as well as allowing a much wider range of simple geometries to be examined.

In a geometry where the electrons do not strike any surface, the trajectories are indefinitely long and it is impossible to calculate the space charge exactly. The in-house program deals with long trajectories by truncating them after a single reflexive trajectory, after which the electron is considered to have returned to the electron distribution around the cathode. It is not possible to use the same method in the commercial program, so the paths are simply truncated outside the far end of the solenoid, after the electrons have completed their outgoing journey. Care is taken to prevent artifacts, such as sudden changes in the computed space charge at points where the electron paths "stop". In both cases, the charge contained

within the ion source is given by the product of the effective cathode emission and the average lifetime of the trajectories. When the total charge in the device is small, the simulations converge satisfactorily. However, as the charge increases we note that the simulations become unstable so that the trajectories, as well as the resulting space charge, begin to oscillate. In such cases, we observe that, after a few iterations, the entry of electrons into the device is partially or totally inhibited by the build up of space charge. The space charge level on the next iteration then drops and the successive iterations fluctuate with no indication of convergence. The effect is as one might expect since there is a maximum charge that can be sustained by emission from the filament. We use the onset of the oscillatory behavior as an indication of the maximum amount of charge the device can carry.

## V. ELECTRON INJECTION INTO THE SOLENOID

We simulate a simple electron source in which the electron emitter is a single, circular coil of wire, placed coaxial with the solenoid. The coil is located in the electrostatic fringing field between the liner (at potential $V_L$) and the surroundings (the background region is held at 0 V; see Fig. 4). The fringing field extracts electrons from the filament and accelerates them to the required energy. Apart from the simplicity of this arrangement, another benefit is that with suitable magnetic confinement of the trajectories, electrons cannot reach other electrodes, in contrast to alternative designs (11; 12). Thus, electron loss mechanisms can be extremely low and a large space charge can be achieved even at low emission currents.

Calculations of the maximum charge that the device can hold in a reflexive mode are performed with the in-house numerical simulation and are shown in Fig. 5 as a function of the filament position. We define the operation as being in reflexive mode if more than 90% of the trajectories return to the filament after propagating through the liner. Each panel in the figure corresponds to a particular potential (between 600 V and 800 V) of the filament, with the liner fixed at 1000 V. Thus, the panels correspond to nominal electron energies of (a) 400 eV, (b) 300 eV and (c) 200 eV. The maximum charge in the device, for a given position of the filament, is shown by the shading/color of the pixel corresponding to that filament position.

Figure 5 shows that reflexive operation only occurs in the small colored regions and that most pixels do not support reflexive trajectories. We consider the non-reflexive region first. Here there are significant loss mechanisms: for example, electrons hitting an electrode or failing to enter the device. An examination of the trajectories shows that the non-reflexive regime can be divided into three sub-regions, labeled **A**, **B** and **C** in Fig. 5. In region **A**, the filament potential is significantly higher than the surroundings and there is insufficient electrostatic field to extract electrons in any direction from the filament. Trajectories from region **B** have a significant probability of striking the liner, either at its left or right extremity. Such trajectories are lost and do not contribute to a reflexive mode of operation. In region **C**, the filament potential is significantly lower than that of the surrounding volume. The field therefore extracts electrons from the filament in all directions. Trajectories arising from the front (right side in Fig. 5) of the filament execute reflexive trajectories; however, trajectories starting from the rear of the filament propagate away from the liner before reversing their direction. It is these latter trajectories that do not contribute to full reflexive motion: in general, they have large pitch angles with respect to the local magnetic field and they are therefore reflected by the converging **B**-field (the "magnetic mirror" effect in which particles initially traveling at an angle $\beta$ to magnetic field lines of strength $B_0$ will be reflected if the field rises in strength to $B_{\rm crit} = B_0(1+\cot\beta)^2$ (18)). Such trajectories add to the space charge near the filament but they do not propagate into the ionization region sufficiently to contribute to efficient ionization. The exact shape of regions **A**, **B** and **C** depends on the criterion we use to define reflexive operation; however, the results indicate clearly that there is an optimum position for the filament, which will result in low electron loss and where the electron motion is almost exclusively reflexive.

We now discuss the colored region, when the motion is predominately reflexive. Note that, in all cases, the reflexive region spans only a few millimeters. For example, a potential of 800 V [Fig. 5(c)] gives an optimum charge when the filament is sited between approximately 5 mm and 2.5 mm from the entrance to the liner. When the potential is 600 V [Fig. 5(a)], the corresponding region is further to the left, between approximately 7.5 mm and 3.5 mm from the entrance to the liner. The behavior can be understood from the competition of loss mechanisms identified in the discussion of regions **A** and **C**, above. If the filament is too close to the liner, electrons are reflected in the converging magnetic field without entering the liner. In contrast, if the filament is too far from the liner, no electrons are extracted from the filament. The optimum position clearly depends on the local electric field at the filament. Contours of constant electrostatic potential, in the absence of the filament and space charge but including the filament mount (**9**, in Fig. 4), have been superimposed on Fig. 5. The isopotentials indicate a useful rule-of-thumb; namely, that the filament should be placed at a point where, in the absence of the filament, the potential is between 50 V and 100 V higher than the desired filament potential. Such a position gives a strong extraction field and one that favors trajectories propagating towards the liner with small pitch angles.

Figure 5 also shows that there is an optimum radius for the filament. The charge held by the device increases with the filament radius for all positions along the axis. Beyond a certain point, however, the charge drops drastically as the radius is increased and region **B** is entered. The behavior can be understood from the contribution of the space charge to the available volume element in the cylindrical system. Emission from the filament ceases when the space charge reduces the extraction field to zero and the charge required to achieve that end increases linearly with the radius of the loop. The optimum radius is then the largest value possible before the onset of electron loss in region **B**.

The above results help to explain the extreme sensitivity to cathode position observed previously (12) and show that the

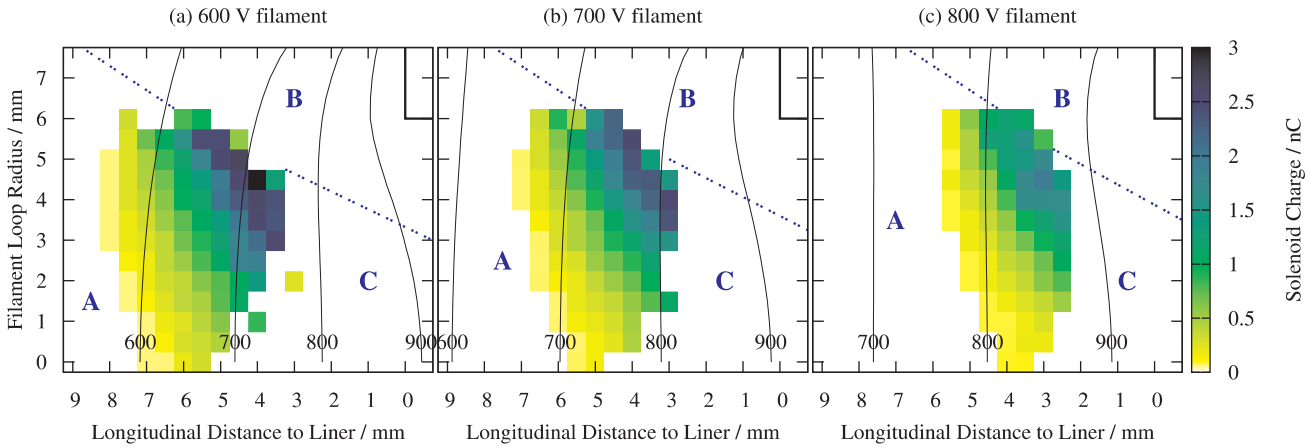


FIG. 5 [Color online] The effect of filament position on the charge held by the ion source, for the optimum trajectory region where 90% of all trajectories are reflexive. For each position of the filament, on a square 0.5 mm grid, the maximum charge held within the ion source is shown as a color for three potentials on the filament and its mount (panels a–c). Also shown is the boundary of the solenoid liner (thick solid line in upper right corner) and the electric isopotentials (thin solid lines) when both the filament and space charge, though not the filament holder, are absent from the simulation. The solenoid liner potential is 1000 V throughout and the filament is at (a) 600 V, (b) 700 V and (c) 800 V. Trajectories are included in the optimum region when they are stable over a large number of iterations and have at least 90% of the trajectories performing many traversals of the solenoid core. The background of zero-valued pixels can be sub-divided into three regions, labeled **A**, **B** and **C** and separated by dotted (blue) lines (see text). The simulation geometry used is as described in Fig. 6(a).

correct filament position is critical to obtain an ideal, reflexive mode of operation. Fortunately in a real device, providing the filament is sited close to the optimum position, its potential can be adjusted to fine tune the system. Specifically, the results show that operation of a very long ion source (300 mm in the present case) is possible. In reflexive mode there is minimal electron loss and the emission current simply provides for the remaining loss mechanisms that exist.

## VI. ION EXTRACTION FROM THE SOLENOID

Efficient extraction of ions from the ion source is necessary not only to obtain the best sensitivity but also to reduce the residence time of ions in the ionization region and to minimize the degree of multiple ionization. We have shown that the electron space charge hinders ion extraction by creating potential barriers at both ends of the solenoid (see Fig. 3). In the present section we discuss some strategies to engineer these barriers so as to improve ion extraction.

Figure 6(a) shows the basic configuration we have discussed so far. The upper panel shows the electrodes, electron trajectories and solenoid, while the lower panel shows the axial potential both with and without electron space charge. The bold line indicates the axial potential in the presence of electron space charge; the shaded area, which lies between the dashed line and the axial potential, shows the range of potential in which ions are created.

In the absence of space charge the axial potential is close to the liner potential, 1000 V, except at the ends, where it falls rapidly to 0 V. In the presence of space charge, the axial potential is approximately 900 V, indicating that the space charge gives a potential well of 100 V [Fig. 6(a)] whilst the potential barrier at each end is approximately 40 V, which is sufficient to trap ions created with thermal energies. The data in Fig. 6(a) confirm the qualitative arguments given in Section II. The simulations indicate a clear annular form to the electron beam and, although the volume charge density within the beam varies with radius, typical equivalent values for $\alpha$ range between 0.75 and 0.85. Figure 6(a) also shows that the barriers at the entrance and exit are of a similar magnitude so that there is nothing to favor extraction in a specific direction.

Figure 6(b) includes the two modifications to the geometry that were present in the experimental prototype discussed in Section III. First, a barrier ring is included to prevent ions emerging to the left, and second, an extraction tube is added to facilitate extraction toward the right. The barrier ring is inserted nearer the entrance than in the prototype, where it minimizes the width of the barrier. The effect on the axial potential near the entrance is shown by comparing the lower panels in Fig. 6. With the barrier ring in place, the entrance barrier increases by approximately 30 V and it will always be energetically favorable for ions to emerge from the exit (right) side. For the simulation shown in Fig. 6(b), the extraction tube is set at 920 V with respect to ground potential; that is, 80 V lower in potential than the liner. The extraction tube suppresses the electrostatic potential sufficiently to eliminate the barrier caused by the electron space charge. Thus, most of the ions created in the main body of the ion source have sufficient energy to emerge. However, the effect is not ideal since a small, deep well is created near the exit. Since ions created in that region cannot emerge spontaneously, their residence time in the ion source will be significant. Furthermore, some of the ions created in the main body of the solenoid will also be trapped since the axial magnetic field increases towards the center of the solenoid where there is a corresponding minimum in the electrostatic potential. The effect is much smaller than the barriers at each end of the solenoid but is significant

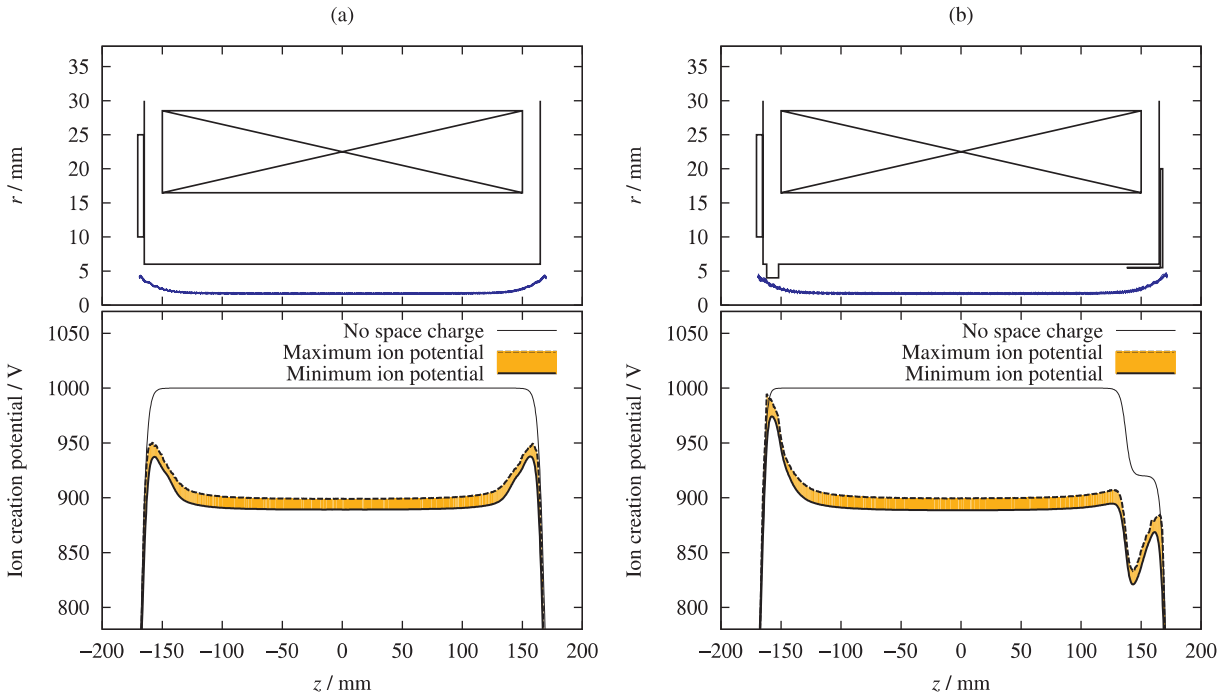


FIG. 6 [Color online] Ion creation and extraction in a solenoid ion source of nominal length 300 mm. The upper panels show the solenoid geometry and the simulated electron trajectories (blue lines). The lower panels show the corresponding electrostatic potential on the axis, both with and without the electron space charge (solid lines) as in previous figures. (a) A uniform solenoid winding pattern with a cylindrical liner. (b) The same geometry but with an ion barrier ring (left) and ion extraction tube (right) similar to those of the experimental prototype. The liner, from $-165$ mm $< z <$ 165 mm with inner radius 6 mm, has a potential of 1000 V; the cathode (at the leftmost edge of the electron trajectories) and mount, from $-170.5$ mm $< z < -165.5$ mm, with inner radius 10 mm, have a potential of 700 V. In (b) there is also an ion barrier ring, from $-162$ mm $< z < -152$ mm, with inner radius 4 mm, at the liner potential; and an ion extraction tube from 138 mm $< z <$ 168 mm with inner radius 5.5 mm and a potential of 920 V. The charge held within the solenoid is 1.71 nC in (a) and 1.88 nC in (b). The magnetic field strength at (z = 0, r = 0) is 150 mT and is generated from a series of ten simple solenoids, all in the region $-150$ mm $< z <$ 150 mm. The radius of the innermost coil is 16.48 mm and layers are linearly spaced in $r$ such that each coil has a radius 1.21 mm larger than the previous coil.

in the context of ions created with thermal energies.

Figure 7 illustrates a number of strategies that further improve the extraction of ions. The aim is, firstly, to engineer the magnetic field to control the electrostatic potential and, secondly, to replace the extractor electrode with a modified liner. A constant electrostatic potential will arise from a more homogeneous magnetic field. Simple correction coils at the entrance and exit of the solenoid, as in the upper panel of Fig. 7(a) achieve the objective. These coils are adjusted to create a magnetic field that is constant to better than 0.32 % within the solenoid. The correction coils also ensure that the transition region from low-field, outside the solenoid, to high-field, inside the solenoid, occurs more quickly. As a consequence, the electrostatic potential in the main body of the device will be constant and the space charge barrier at the exit and entrance will be narrower.

The upper panel in Fig. 7(a) also shows that the extraction tube in Fig. 6(b) is replaced by a tapered exit channel to the liner. As before, the lower panels show the corresponding potentials and, in particular, the shaded area gives the range of energies in which ions are created. Calculations of the fields and electron trajectories were performed using the *LORENTZ2D-EM* package in order to deal more effectively with the complicated geometry. However, the longer calculation times meant that a smaller number of trajectories were used in these simulations, with the result that some statistical noise can be seen in the electrostatic potential resulting from the electron space charge. Comparison with Fig. 6(b) demonstrates that there is now no barrier to prevent ion extraction at the right (exit) side. The design shown in the upper panel of Fig. 7(a) achieves the main objective of removing any well to trap ions; however, it does not actively extract ions from the main body of the device. Thus, an ion having an initial velocity in the negative z-direction will travel away from the exit until it is reflected by the potential barrier at the left of the figure before traversing the full length of the ion source and making an exit to the right.

Figure 7(b) illustrates how the magnetic field can be further tailored to achieve active extraction to the right. The geometry is the same as in Fig. 7(a) except that the magnetic field is designed to increase continuously throughout the main body of the device. The stronger field draws the electron beam closer to the axis and the space charge depresses the electrostatic potential. The desired field is achieved by maintaining a constant current density in the solenoid while decreasing the inner diameter of the solenoid linearly throughout its length. A good

approximation to such a field could be obtained, in practice, by adjusting the winding pattern and/or adding a number of further correction coils. Inspection of the lower panel in Fig. 7(b) demonstrates that the electrostatic potential has a constant gradient and gives an extraction field of approximately 100 V/m under the conditions in the simulation. Thus, an ion moving initially to the left with thermal energy will reverse its direction after moving an axial distance of less than 1 mm. There is a corresponding increase in the spread of ion energies, which can be estimated from the figure. The main ionization region extends from $-140$ mm $< z <$ 110 mm. Over that region, the 100 V/m extraction field adds a modest energy spread of 25 V.

## VII. DISCUSSION

The results in section VI demonstrate that careful engineering of both the magnetic field and the geometry gives efficient ion extraction. The analysis of electron injection into the solenoid indicates that the filament position is critical to achieve a high fraction of reflex trajectories, enabling operation in a regime where a high electron density can arise from a relatively small emission current. The benefit of a low emission current is that the filament power is correspondingly small so that degassing is reduced. In any ionizer the background gas contributes to the total ion production and it follows that minimizing the degassing rate is a desirable objective.

A device that operates with high electron density but low emission current is qualitatively different from the conventional Brink or Weiss designs. In the original work of Weiss(6), a large electron density was used to give high ionization efficiency and also to facilitate ion extraction. However, the emission current was very large, which required a high power filament. Electron space charge plays a more complex role in designs of the Brink type. The extraction of ions is affected at low current densities before there is a significant effect on the electron emission(19). Space charge can reduce the overall efficiency(19) as well as lead to nonlinearities arising from ion trapping and the accumulation of ion space charge(20). The effects are particularly important in applications, such as gas analysis, where only a small range of ion energies can be tolerated.

It is a general rule that the spread of ion energies emerging from a source cannot be less than the variation in potential across the electron beam due to space charge. Thus, increasing the ionization efficiency by raising the electron density generates a larger energy spread in the ions. There is necessarily a limit on the acceptable energy spread imposed by the subsequent mass selection, which suffers from chromatic effects in the ion optics. Consequently, the overall efficiency of an ion source is determined by the sensitivity of the ion optics to chromatic aberration and, in any design, efficiency cannot be increased indefinitely simply by increasing the electron density. Instead, the approach in the present paper achieves high performance by exploiting the primary advantages of the solenoidal geometry; namely, the combination of a high ionization efficiency and a ionization region whose length can be extended almost indefinitely, yielding a volume orders of magnitude larger than in previous devices.

## References


[1] I. G. Brown. *The Physics and Technology of Ion Sources*. Wiley, 1989.

[2] P. Fouquet, A. P. Jardine, S. Dworski, G. Alexandrowicz, W. Allison, and J. Ellis. *Rev. Sci. Instrum*, 76(5):053109, 2005.

[3] D. A. MacLaren and W. Allison. *Inst. Phys. Conf. Ser.*, 179:383–388, 2004.

[4] D. Bassi. In Giacinto Scoles, editor, *Atomic and molecular beam methods*, volume 1. Oxford University Press, 1988.

[5] A. O. Nier. *Rev. Sci. Instrum*, 11(7):212–216, 1940.

[6] R. Weiss. *Rev. Sci. Instrum*, 32(4):397–401, 1961.

[7] G. O. Brink. *Rev. Sci. Instrum*, 37(7):857–860, 1966.

[8] C. J. Park and J. R. Ahn. *Rev. Sci. Instrum*, 77(8):085107, 2006.

[9] O. Ameziane, J. M. Blanco, J. J. Serrano, B. Guzmán, and M. Aguilar. *Eur. Phys. J. AP*, 22(3):231–235, 2003.

[10] B. Brutschy and H. Haberland. *J. Phys. E: Sci. Instr.*, 10(1):90–94, 1977.

[11] M. DeKieviet, D. Dubbers, M. Klein, U. Pieles, and C. Schmidt. *Rev. Sci. Instrum*, 71(5):2015–2018, 2000.

[12] A. V. Kalinin, L. Yu. Rusin, and J. P. Toennies. *Inst. Exp. Tech.*, 49(5):709–713, 2006.

[13] B. Yue, E. D. Lee, A. L. Rockwood, and M. L. Lee. *Anal. Chem.*, 77(13):4160–4166, 2005.

[14] B. Yue, E. D. Lee, A. L. Rockwood, and M. L. Lee. *Anal. Chem.*, 77(13):4167–4175, 2005.

[15] E. D. Donets, E. E. Donets, R. Becker, L. Liljeby, K.-G. Rensfelt, E. N. Beebe, and A. I. Pikin. *Rev. Sci. Instrum*, 75(5):1566–1568, 2004.

[16] E. D. Donets, E. E. Donets, and D. E. Donets. *Rev. Sci. Instrum*, 73(2):696–698, 2002.

[17] Integrated Engineering Software. `http://www.integratedsoft.com/products/Lorentz.aspx`.

[18] T. J. M. Boyd and J. J. Sanderson. *Plasma Physics*. Thomas Nelson and Sons Ltd., 1969.

[19] M. C. Cowen, W. Allison, and J. H. Batey. *Meas. Sci. and Technol.*, 4(1):72–78, 1993.

[20] M. C. Cowen, W. Allison, and J. H. Batey. *J. Vac. Sci. Technol. A*, 12(1):228–234, 1994.

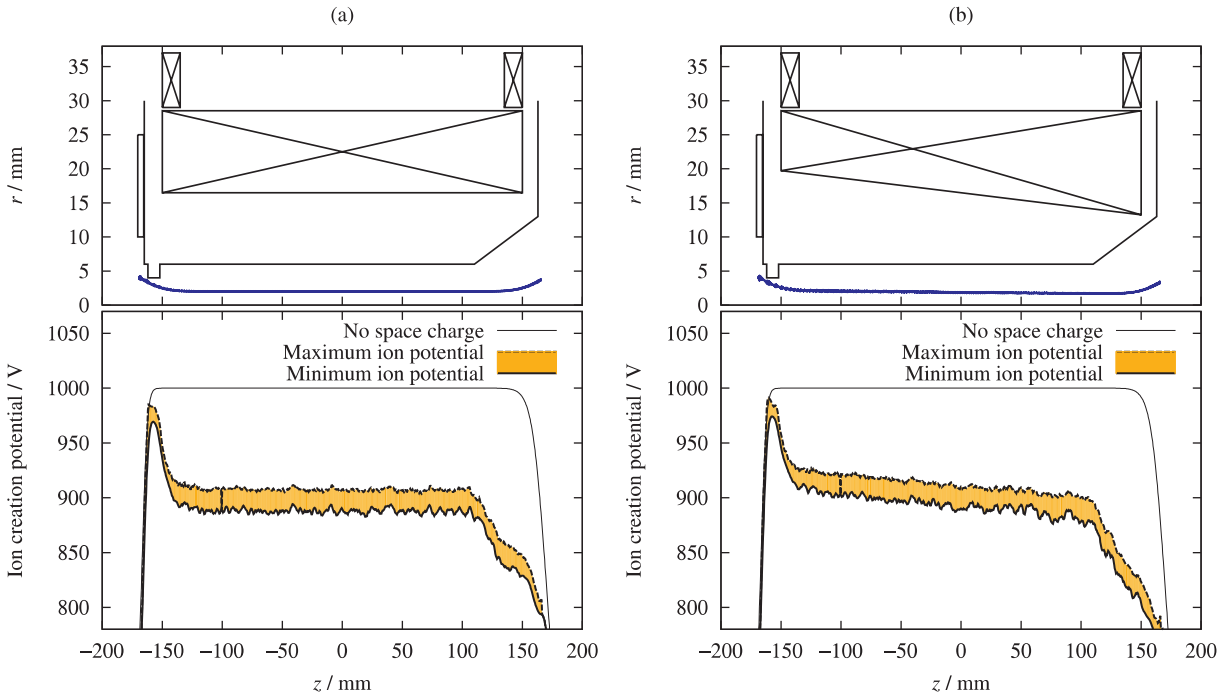


FIG. 7 [Color online] As in Fig. 6 but with modifications to the field and liner. (a) A uniform solenoid winding pattern with correcting coils at each end and a tapered exit channel in the liner. (b) The same geometry but with a uniform magnetic field gradient. The liner radius increases linearly to 13 mm starting at $z = 110$mm; the correction coils have a length of 15 mm, inner radius 29 mm, outer radius 37 mm, and current density of $10^7$ A m$^{-2}$. The main solenoids have the same dimensions at $z = 0$ *mm* as in the previous figure; in (a) it is uniformly thick and in (b) it has a linear thickness variation of $\sim 6.5$ mm. The total charge held within the solenoid is 2.24 nC in (a) and 1.70 nC in (b), the difference arising from the particular choice of magnetic field geometry in each panel. The magnetic field strength at (z = 0, r = 0) is 150 mT in both (a) and (b).